Petroleum Science 21 (2024) 3558–3574

Contents lists available at ScienceDirect

Petroleum Science

journal homepage: www.keaipublishing.com/en/journals/petroleum-science

Original Paper

Influence of the mechanical properties of materials on the ultimate pressure-bearing capability of a pressure-preserving controller

Xiao-Jun Shi [a], He-Ping Xie [a, b], Cong Li [a, *], Gui-Kang Liu [a], Zi-Jie Wei [a], Tian-Yu Wang [a], Ju Li [c], Qiu-Yue Li [d]

[a] State Key Laboratory of Intelligent Construction and Healthy Operation and Maintenance of Deep Underground Engineering, College of Water Resource and Hydropower, Sichuan University, Chengdu, 610065, Sichuan, China
[b] Guangdong Provincial Key Laboratory of Deep Earth Sciences and Geothermal Energy Exploitation and Utilization, Institute of Deep Earth Sciences and Green Energy, College of Civil and Transportation Engineering, Shenzhen University, Shenzhen, 518060, Guangdong, China
[c] College of Mechanical Engineering, Sichuan University, Chengdu, 610065, Sichuan, China
[d] Jinshi Drilltech Co. Ltd., Tangshan, 063004, Hebei, China

ARTICLE INFO

Article history:
Received 6 May 2023
Received in revised form
22 February 2024
Accepted 8 April 2024
Available online 10 April 2024

Edited by Jie Hao and Meng-Jiao Zhou

Keywords:
In-situ pressure-preserving coring
Pressure-preserving controller
Material properties
Ultimate pressure-bearing capability

ABSTRACT

The pressure-preserving controller is the core part of deep in-situ pressure-preserving coring (IPP-Coring) system, and its pressure-preserving capability is the key to IPP-Coring technology. To achieve a good understanding of the influence of mechanical properties of materials on the ultimate pressure-bearing capability (UPB-Capability) of the pressure-preserving controller, the IPP-Coring experimental platform was developed to test the UPB-Capability of pressure-preserving controllers of four different materials. The experimental results show that the UPB-Capability of pressure-preserving controllers with different material varies greatly. A numerical model of the pressure-preserving controller was developed to study the influences of mechanical parameters of materials on the UPB-Capability of the pressure-preserving controller after the accuracy of the numerical model is verified by experiments. The results indicate that the yield strength (YS) and Poisson's ratio (PR) of the material have little effect on the UPB-Capability of the pressure-preserving controller, whereas the elastic modulus (EM) of the material has a significant effect. A generalized model of the UPB-Capability of the pressure-preserving controller is developed to reveal the mechanism of the influence of material properties on the UPB-Capability of the pressure-preserving controllers. Considering these results, the future optimization direction of the pressure-preserving controller and material selection scheme in practical engineering applications of the pressure-preserving controller are suggested.

1. Introduction

As the Earth's shallow resources are mined out, the development of resources to go deeper (Gao et al., 2021b; Kong et al., 2023; Xie et al., 2021b, 2022). The initial pore pressure of deep rocks has a considerable effect on the in-situ mechanical characteristics of rocks (Ma et al., 2023; Shen et al., 2022; Zhao et al., 2022). The changes of initial pore pressure will cause the changes of internal microstructure of deep rocks, which will further lead to the porosity and permeability of rock change obviously and the strength and deformation properties are considerably changed (Bhakta et al., 2016; Ren et al., 2021; Sun et al., 2023). However, most of the existing studies on deep rock characteristics are based on the “ordinary core” under the conditions of unrealistic store environment -and released pore pressure (Gao et al., 2021b, 2022; Li et al., 2023; Xie et al., 2023b), which obtain the basic physical and mechanical characteristics of rock materials and ignore the effect of initial pore pressure on rock properties, extremely limiting the significance of engineering guidance and seriously threaten the safety and efficiency of deep resource mining (Shi et al., 2023; Xie et al., 2019, 2022). Therefore, to develop deep resources, it is necessary to obtain deep in-situ pressure-preserving core samples and develop deep in-situ rock mechanics theory (Xie et al., 2020, 2021a, 2023a).

* Corresponding author.
E-mail address: licong@scu.edu.cn (C. Li).

https://doi.org/10.1016/j.petsci.2024.04.003

To obtain deep in-situ pressure-preserving core samples, a series of pressure-preserving corers have been developed by various countries (Abegg et al., 2008; Chen et al., 2013; Hu et al., 2022; Qin et al., 2016; Sukumar et al., 2015; Zhu et al., 2013). Most pressure-preserving corers use pressure-preserving controllers (ball valves or flap valves) as pressure-preserving sealing mechanisms (Burger et al., 2003; Gao et al., 2021a; Guo et al., 2023; Kawasaki et al., 2006). The ultimate pressure-bearing capability (UPB-Capability) of the pressure-preserving controller determines the upper limit of a pressure-preserving coring technology (Li et al., 2021). The pressure core sampler (PCS) with the best pressure-preserving performance adopts a ball valve as the pressure-preserving sealing mechanism, with a UPB-Capability of 70 MPa, and a field application that does not exceed 35 MPa (Pettigrew, 1992). The ball valve can easily be jammed during the closing process and not seal effectively, resulting in a low pressure-preserving success rate (Wu et al., 2016). Compared with a ball valve, a flap valve can achieve a self-tightening seal while obtaining a larger core diameter, which is more suitable for deep in-situ pressure-preserving coring (IPP-Coring) (Guo et al., 2023). However, existing flap valves have a pressure-preserving capacity of less than 30 MPa (Hohnberg et al., 2003; Hu et al., 2022; Qin et al., 2005), which is far from meeting the needs of deep resource exploration and development. Therefore, to maximize the coring diameter within the annular assembly space of the coring tool, as well as to enhance the UPB-Capability of the pressure-preserving controller, Li et al. proposed five pressure-preserving controller structures based on the Steinmetz solid principle (He et al., 2019; Li et al., 2021, 2022a, 2022b; Liu et al., 2020; Wu et al., 2020), as shown in Fig. 1. However, even when using the same pressure-preserving controller structures, the UPB-Capability varies considerably if the materials are different. On the one hand, changes in the YS, EM and other material parameters will directly lead to changes in structural strength and stiffness (Jackson and Green, 2005; Wei et al., 2015). On the other hand, changes in these parameters will also change the size of the crack tip opening displacement, which will indirectly cause changes in structural strength and stiffness (He et al., 2011; Zhang et al., 2019; Zhang and Cui, 2003). Therefore, a reasonable choice of materials is a prerequisite for optimizing external pressure components performances (Zhang, 2018).

Wang et al. (2021) noted that the pressure-preserving sampler not only has requirements for thermodynamic material properties but also needs to consider the ultimate pressure-bearing strength and seawater corrosion resistance. They listed several metal materials commonly used for corers, such as 0Cr17Ni4Cu4Nb stainless steel, 40Cr alloy steel and TC4 titanium alloy. Li et al. (2022b) found that the material characteristics of a valve have a significant effect on the contact characteristics of a rough surface based on the microcontact theory of rough surfaces, and the sealing performance can be improved to a certain extent by selecting materials with a low elastic modulus. Jackson et al. (2017) developed a MAC-EXP system to recover deep-sea sediments in an in-situ environment. Most corer parts were manufactured using 316 (A4) grade stainless steel, but electrochemical processes in the stainless steel caused oxygen to be consumed in the core chamber during application. Wang et al. (2022) developed a thin-walled pressure-preserving coring tool to meet the strength requirements under working conditions, and the material chosen was 45MnMoB. Huang et al. (2023) developed a pressure-preserving corer in deep coal mines, and Guo et al. (2022) developed a sediment pressure-preserving sampler for deep-sea applications; considering the corrosion resistance of the material and strength requirements, the material chosen was 17-4 PH stainless steel. Garel et al. (2019) developed a microbial pressure preservation sampler for deep-sea use; Chen

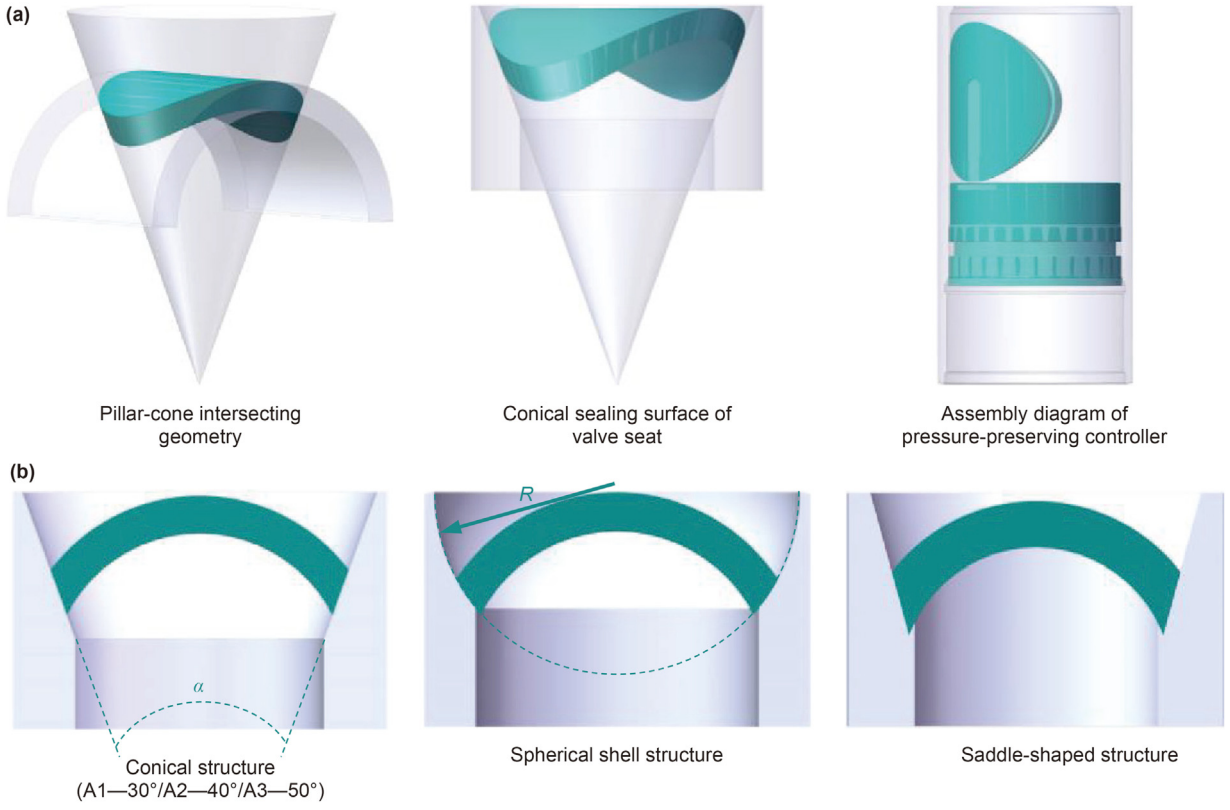

Fig. 1. The pressure-preserving controller: **(a)** design principle and **(b)** five configurations.

et al. (2017) developed a pressure-retaining sampler for deep-sea sediment; Wu et al. (2010) designed a high-pressure cone valve for deep-sea gas-tight water samplers; He et al. (2023) designed a submersible-mounted sampler capable of collecting pressure-preserving samples at a full ocean depth; the material chosen for these devices was titanium alloy because of its low density, high tensile strength, and good resistance to seawater corrosion. Liang et al. (2023) carried out tensile tests on 304 stainless steels at different temperatures and studied the pressure-bearing characteristics of pressure-preserving controllers under temperature and pressure conditions. Their results showed that 304 stainless steel has stable mechanical properties and is suitable for use as a material for pressure-preserving controllers in high-temperature environments. It can be seen that for existing pressure-preserving controllers or sampling systems, the selection of materials mainly considers the mechanical properties of the material and the environmental application. The choice of materials is very wide, but the mechanical properties of the material on the ultimate pressure-bearing capability of the pressure-preserving controller are not clear, which leads to the lack of information for the material selection scheme of pressure-preserving controllers in practical engineering applications. A pressure-preserving controller operates under ultrahigh pressure, high temperature and strong corrosion conditions for a long time and is subject to both environmental or media corrosion and complex stress loads, which is likely to lead to the failure of the coring task due to unreasonable material selection, which is inconsistent with its high deployment cost.

Thus, in this study, both experimental and numerical studies are conducted on the influence of the material mechanical properties on the UPB-Capability of A1 pressure-preserving controllers. In

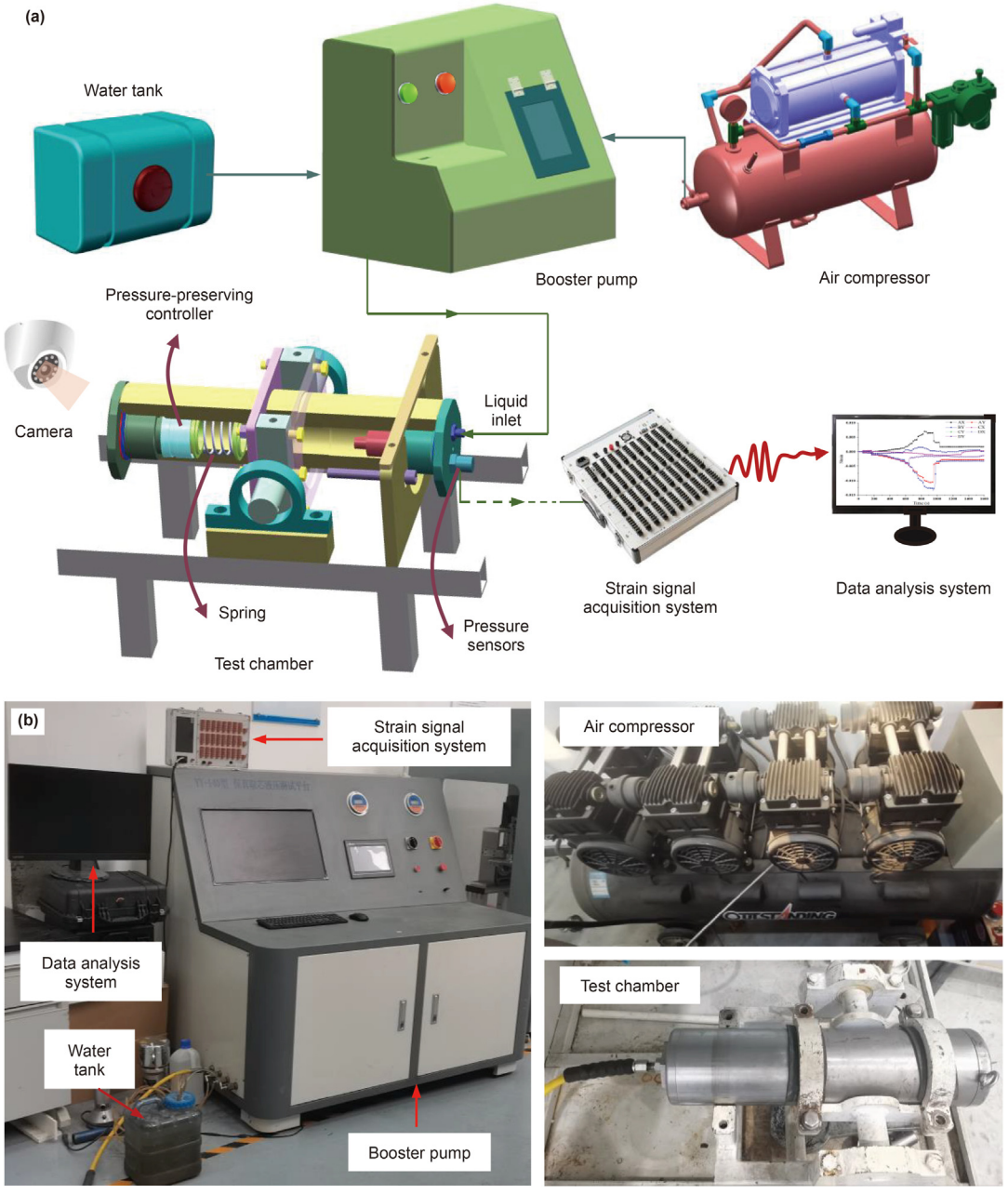

Fig. 2. The IPP-Coring experimental platform: **(a)** schematic diagram and **(b)** photographs.

addition, a general model of the UPB-Capability of the pressure-preserving controller is established, and the future optimization directions and a material selection scheme for a pressure-preserving controller in practical engineering applications are proposed. The remainder of this paper is structured as follows. In Section 2, the experimental and numerical methods are introduced. In Section 3, experimental and numerical simulation results on the effect of material mechanical parameters on the UPB-Capability of a pressure-preserving controller are presented in detail; this is followed by a comprehensive discussion on the influence mechanisms in Section 4. The results are summarized in Section 5.

2. Experimental and numerical methods

2.1. Experimental apparatus and test procedure

To test the UPB-Capability of pressure-preserving controller, the in-situ pressure-preserving coring experimental platform was developed (Fig. 2). The platform can perform pressure tests under conditions of 0–140 MPa and monitor pressure changes. The experimental device mainly includes a booster pump, water tank, strain signal acquisition system, data analysis system, air compressor, and test chamber. The booster pump is composed of two sets of high-precision servo-controlled thrust oil sources with infinite total volume-boosting and voltage-stabilizing functions. The air compressor converts the atmosphere into compressed air, which provides a working air source for the booster pump. The interior of the test chamber constitutes the test space to complete the pressure-preserving controller pressure-preserving capacity test. The strain signal acquisition system can monitor the deformation characteristics of the pressure-preserving controller in real time. The data analysis system can analyse and process all the collected raw data to provide data support for the structure and material optimization of the pressure-preserving controller. Table 1 shows the model and related parameters of the experimental equipment.

In this study, four materials, 304 stainless steel, 18Ni, 35CrNi3-MoVR (abbreviated as 35C), and AerMet100 (abbreviated as A100), were selected to test the UPB-Capability of the pressure-preserving controller, and the bonding position of the strain gauge is shown in Fig. 3.

The pressure-preserving controller was first placed on the test chamber outlet, and the initial sealing force was provided by a pretensioned spring pressed against the pressure-preserving controller. The water is pumped into the test chamber by the booster pump through the pipeline and the liquid inlet until a leak occurs in the pressure-preserving controller. The data recorded by the pressure sensor, the strain signal acquisition system and the high-speed camera are transferred via data lines to a computer for storage and related processing.

2.2. Numerical simulation method

According to the self-developed pressure-preserving controller structure, which is appropriately simplified, the numerical model of the pressure-preserving controller is established. The meshing diagram of numerical model is shown in Fig. 4. The contact is defined as a face-to-face contact, the contact attribute is Coulomb friction, the tangential behaviour is a penalty function, the friction factor is 0.2, and the normal behaviour is hard contact. The valve seat is defined as the contact master surface, and the valve cover is defined as the contact slave surface (see Fig. 5(a) and (b)). The load application case is a uniform load applied on top of the valve cover and the boundary condition is that the bottom of the valve seat is completely fixed (Fig. 5(c)).

Numerous studies have shown that the magnitude of contact pressure is critical in assessing the sealing ability of seals. For example, Xie et al. (2015) considered the contact pressure of the sealing surface as one of the most important parameters to evaluate the sealing performance of the blade. Belforte et al. (2018) pointed out the importance of studying the contact properties at the rubber-metal interface, since the contact pressure determines good or bad sealing performance. Peng et al. (2021) noted that the contact state along the sealing region directly determines the sealing performance. Zhou et al. (2006) concluded that an O-ring can achieve sealing only when the maximum contact pressure is greater than the sealing medium pressure. In this paper, we estimate the UPB-Capability of the pressure-preserving controller by arranging the measuring line at the weak point and monitoring the contact pressure fluctuation, and the variation in displacement with load at the position of maximum deformation of the valve cover is monitored (Fig. 6).

To exclude the influence of grid on the calculation accuracy, we calculated five grid models with different cell densities: 40768 cells for grid model 1, 101094 cells for grid model 2, 209074 cells for grid model 3, 315492 cells for grid model 4, and 405131 cells for grid model 5. The maximum contact pressure on the monitoring line of the pressure-preserving controller with different grid numbers under the critical load were extracted respectively, and the results were shown in Fig. 7. With the increase of the number of grids, the maximum contact pressure gradually becomes stable. When the number of grids increases from 315492 to 405131, the change in contact pressure does not exceed 1.0%. Therefore, it can be considered that when the number of meshes is greater than 315492, the simulation results are mesh independent.

3. Results

3.1. Experimental results

Fig. 8 shows the test results for the UPB-Capability of pressure-preserving controllers made with different materials. For the 304 stainless steel material pressure-preserving controller at 5, 10, and 15 MPa, there is basically no change in pressure (Fig. 8(a)). When the pressure is loaded to approximately 20 MPa, the pressure-preserving controller fails. The test strain characteristic curve is shown in Fig. 8(e). The compressive strain of AY is the largest, which is -2.0×10^{-2}, and the tensile strain of BX is the largest,

Table 1
Related parameters of the experimental equipment.

Experimental equipment	Parameter	Value
Booster pump	Output flow	0.3 L/min
	Working pressure	≤140 MPa
	Accuracy of pressure stabilization	0.5% FS
Pressure sensor	Range	0–200 MPa
	Sensitivity	2.0 ± 0.5 mV/V
	Operating temperature	−40–250 (Medium temperature MW24Y01H type)

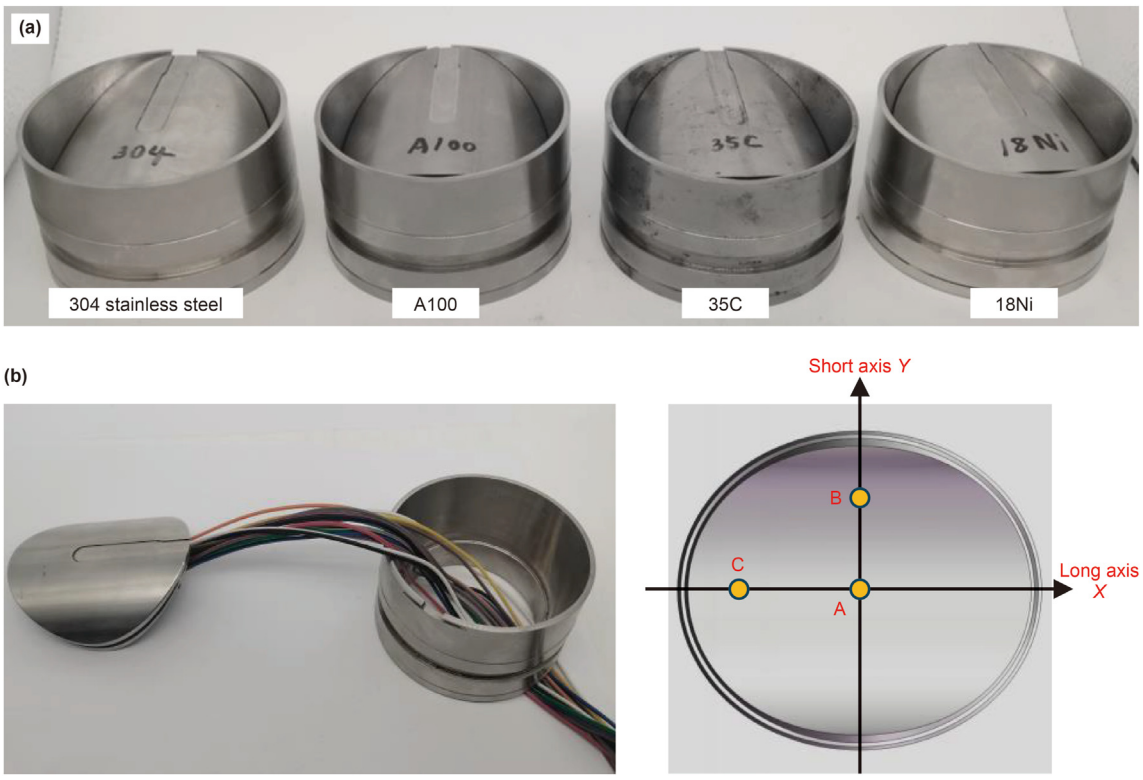

Fig. 3. Basic information of the test sample: **(a)** a photograph of the prepared samples and **(b)** the bonding position of the strain gauge.

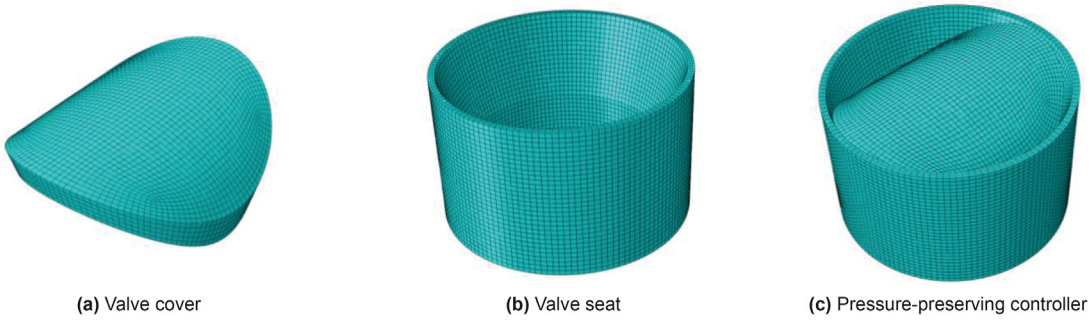

Fig. 4. Meshing diagram of numerical model.

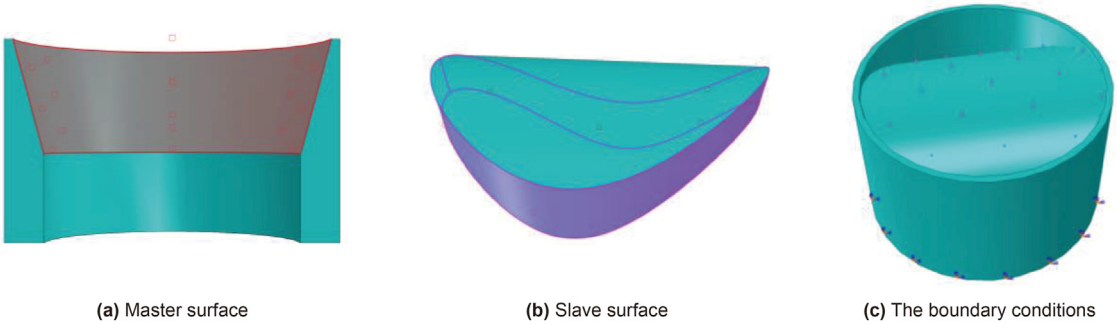

Fig. 5. Seal contact surfaces and boundary conditions.

which is 2.02×10^{-3}. The pressure characteristic curve of the pressure-preserving controller made of 35C material is shown in Fig. 8(b). The pressure-preserving effect is good at 40, 45 and 50 MPa, and there is basically no leakage. When continuing to pressurize to 55.03 MPa, the pressure-preserving controller fails. In Fig. 8(f), as the pressure is stepped up, the strain also changes in a

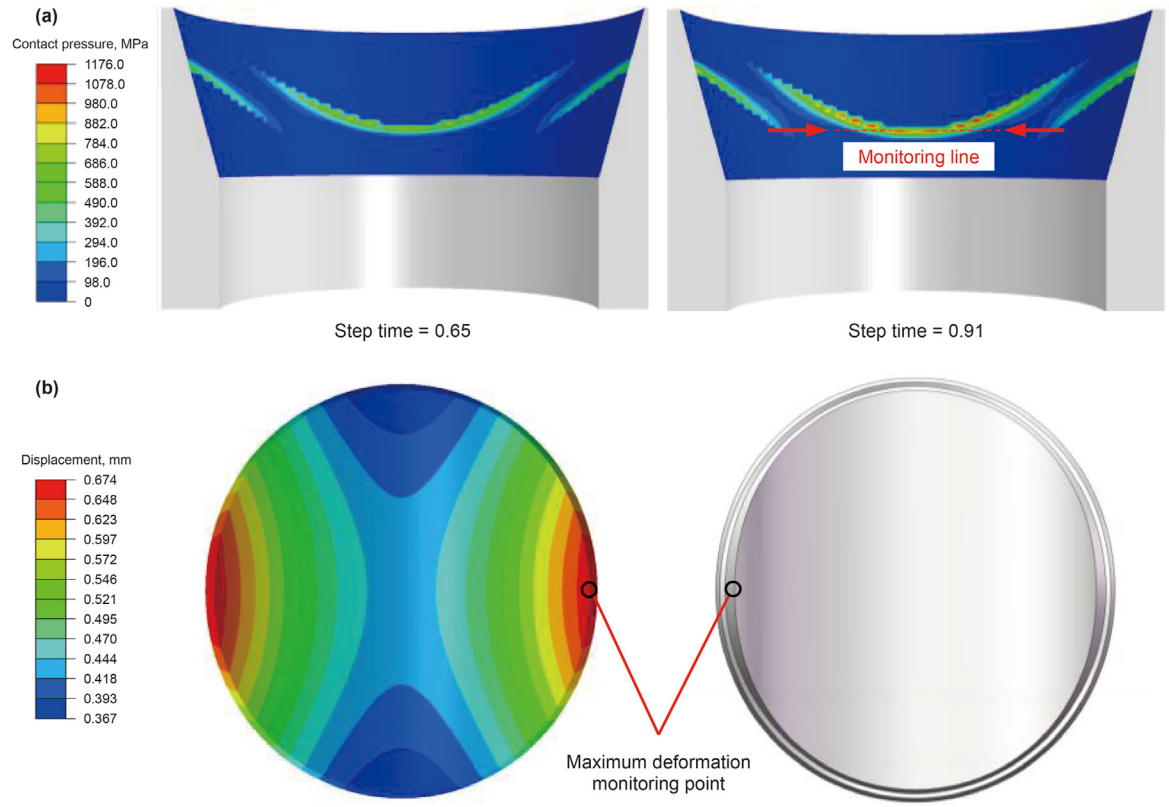

Fig. 6. Monitoring valve cover seal failure: **(a)** contact pressure fluctuations with load increment steps and **(b)** maximum deformation position displacement of valve cover.

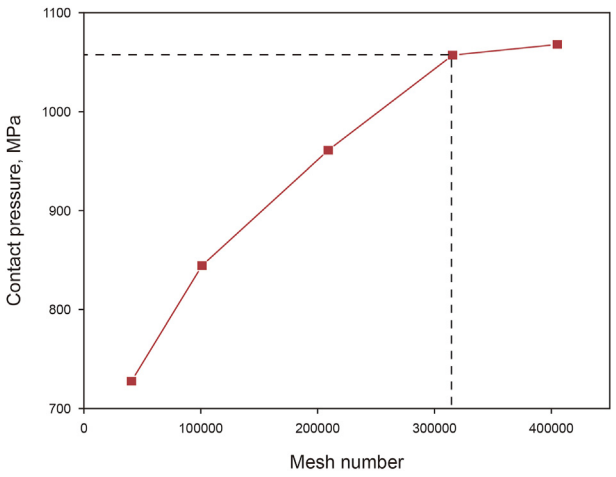

Fig. 7. Results of grid-independence analysis.

stepwise manner, with tensile strain dominating in the *X* direction and compressive strain in the *Y* direction of the pressure-preserving controller. When the pressure increases to 55.03 MPa, the maximum tensile strain in the BX direction is 2.86×10^{-3}, and the maximum compressive strain in the AY direction is -2.37×10^{-2}. Fig. 8(c) shows that the A100 material pressure-preserving controller has a good pressure-preserving effect under 5.25, 10.13 and 15.06 MPa, and there is basically no leakage. When the pressure continues to reach 17.75 MPa, the pressure-preserving controller fails. The test strain characteristic curve is shown in Fig. 8(g). The compressive strain of AY is the greatest at -2.38×10^{-2}, and the tensile strain of BX is the greatest at 2.99×10^{-3}. Fig. 8(d) shows the pressure characteristic curve of the pressure-preserving controller made of 18Ni material. The pressure-preserving effect is good at 5, 10, and 15 MPa. At 22.17 MPa, the pressure fluctuates violently, and if the pressure continues to be applied, the pressure-preserving controller fails. The test strain characteristic curve is shown in Fig. 8(h). The compressive strain of AY is the greatest at -2.96×10^{-2}, and the tensile strain of BX is the greatest at 4.36×10^{-3}.

In general, the pressure-preserving controllers of different materials have good pressure-preserving performance under low-pressure conditions, and the UPB-Capability of pressure-preserving controllers of different materials varies greatly. The UPB-Capability of 35CrNi3MoVR is the highest, at 55.03 MPa, followed by 18 Ni, at 22.17 MPa, and finally 304 stainless steel and A100, at 20 MPa and 17.75 MPa, respectively (Fig. 9).

3.2. Simulation analysis

Since it is difficult to properly assess in the laboratory exactly which parameter is responsible for the variation of the UPB-Capability of a pressure-preserving controller. Often, when one of the material mechanical parameters is changing, the other material mechanical parameters change accordingly. Therefore, to further investigate which material mechanical parameters affect the pressure-preserving controller's UPB-Capability, a numerical model of the pressure-preserving controller was developed using ABAQUS software. After verifying the accuracy of the numerical model, the influence of the YS, EM and PR on the UPB-Capability of the pressure-preserving controller are discussed.

3.2.1. Numerical simulation accuracy verification

To verify the accuracy of the numerical simulation, the same

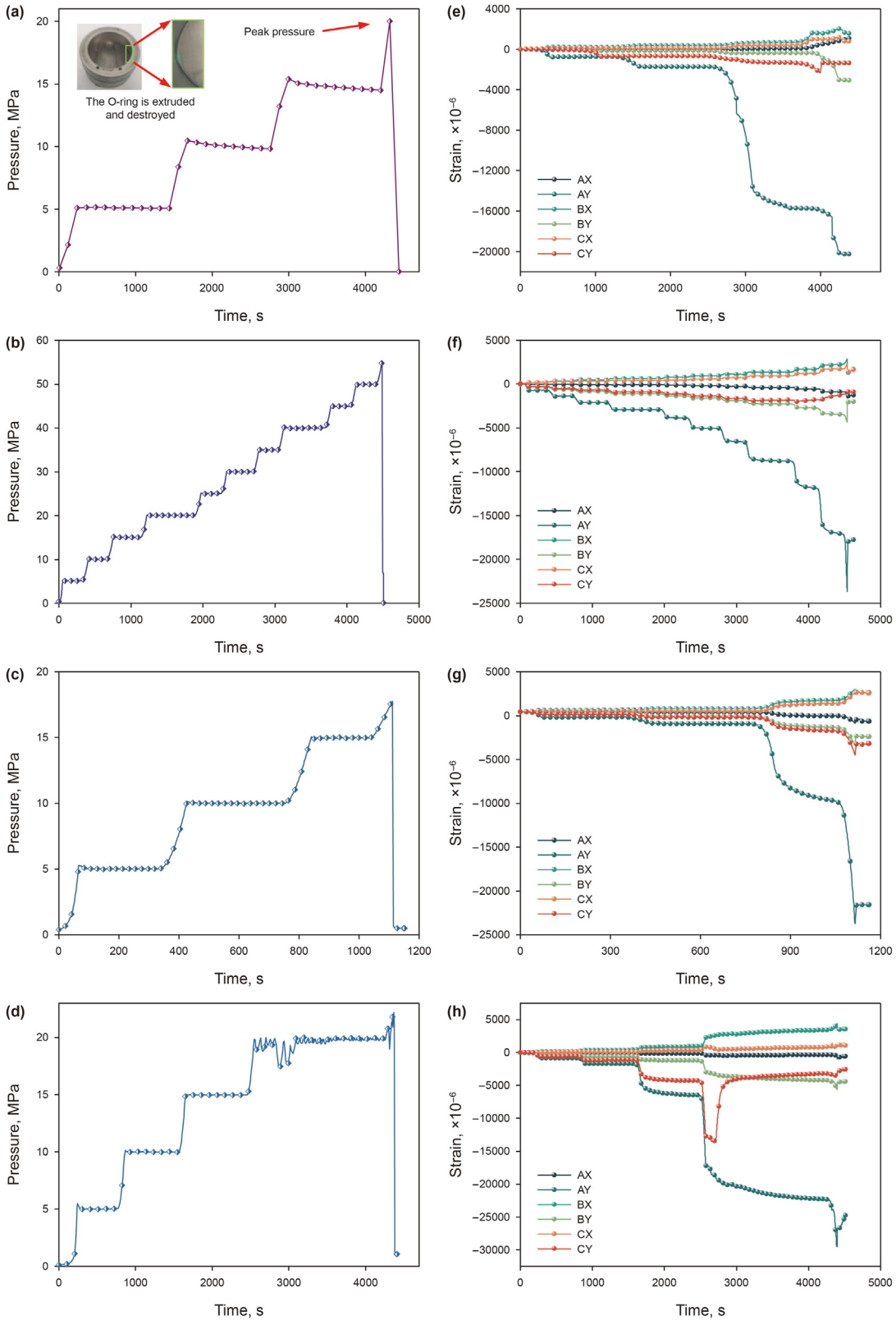

Fig. 8. Pressure curves of pressure-preserving controllers: **(a)** 304 stainless steel, **(b)** 35CrNi3MoVR, **(c)** AerMet100 and **(d)** 18Ni; the strain curves corresponding to different materials of **(e)** 304 stainless steel, **(f)** 35CrNi3MoVR, **(g)** AerMet100 and **(h)** 18Ni.

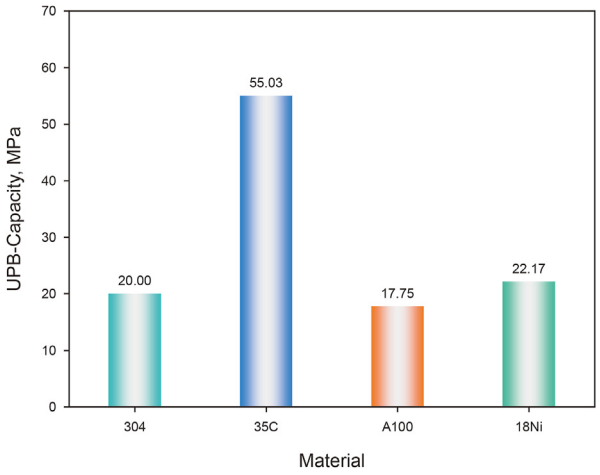

Fig. 9. The test results of the UPB-Capacity of the pressure-preserving controller with different materials.

batch of materials (304 stainless steel and 18Ni materials) of the pressure-preserving controller were processed into standard specimens, which were subjected to tensile tests to obtain the mechanical property parameters, and the tensile test results are shown in Fig. 10. The obtained mechanical parameters were input into the numerical simulation software for analysis, and the change of the contact pressure monitoring curve with load increment on the monitoring line of 304 stainless steel material and 18Ni material was obtained (Fig. 11). Comparing the UPB-Capability of the pressure-preserving controller obtained from the simulation with the test results, it can be found that the error between the simulated results and the experimental results is not more than 5% (Fig. 12). The model chosen in this paper is reasonable and the calculation results are accurate.

3.2.2. Influence of the YS on the UPB-Capability

YS is one of the important indicators to measure the mechanical properties of metal materials. Since the YS of most metals varies widely, considering the material selection of pressure-preserving controllers in practical applications, the YS in this paper is taken as 556, 640, 885, and 1600 MPa, the EM is always taken as 200 GPa, PR is always taken as 0.3, and the model adopts the elastoplastic model. The influence law of the YS on the UPB-Capability of the pressure-preserving controller is studied.

Fig. 13 shows that the change in the monitoring curve of the contact pressure on the monitoring line with the incremental steps of the load under different yield strengths. As the load increases, the contact pressure increases and the middle of the curve becomes progressively concave. According to the numerical simulation estimation method of the UPB-Capability of the pressure-preserving controller, the load with a wide range of contact pressure fluctuation is chosen as the UPB-Capability, and the UPB-Capability of the pressure-preserving controller under different YS conditions is obtained, as shown in Fig. 14.

When the YS are 556, 640 and 885 MPa, the UPB-Capability of the pressure-preserving controllers are 22.2 MPa. When the YS is 1600 MPa, the UPB-Capability is 22.5 MPa. The calculation results show that the YS of the material has little effect on the UPB-Capability of the pressure-preserving controller under critical load conditions because all regions of the pressure-preserving controller are in the elastic deformation stage.

3.2.3. Influence of the EM on the UPB-Capability

The EM is the indicator of the strength of the material's ability to resist elastic deformation under a certain stress, the larger the EM, the smaller the resulting elastic deformation. Since most metals have elastic moduli ranging from 25 GPa to 210 GPa, there is a wide range of variation (Jia and Chen, 2016). The pressure-preserving controller, as the main functional structure, has to ensure that it is applicable to the deep IPP-Coring, which requires a high UPB-Capability. Therefore, the elastic moduli in this paper are taken as 160, 170, 180, 190, 200, and 210 GPa, the PR is always taken as 0.3, and the model adopts the linear elastic model. The influence law of the EM on the UPB-Capability of the pressure-preserving controller is studied. The change in the monitoring curve of the contact pressure on the monitoring line with the incremental steps of the load under different elastic moduli is shown in Fig. 15. Fig. 16 shows that the UPB-Capability of the pressure-preserving controller under different elastic moduli. The UPB-Capability of the pressure-preserving controllers with elastic moduli of 160, 170, 180, 190, 200, and 210 GPa are 21.6, 22.8, 24.3, 25.8, 27.3, and 28.5 MPa, respectively. When PR remains constant, the UPB-Capability of the pressure-preserving controller increases almost linearly with increasing EM. The EM increases by 31.25% from 160 GPa to 210 GPa and the UPB-Capability of the pressure-preserving controller increases by 31.94%. The results indicate that the EM of the material has a significant effect on the UPB-Capability of the pressure-

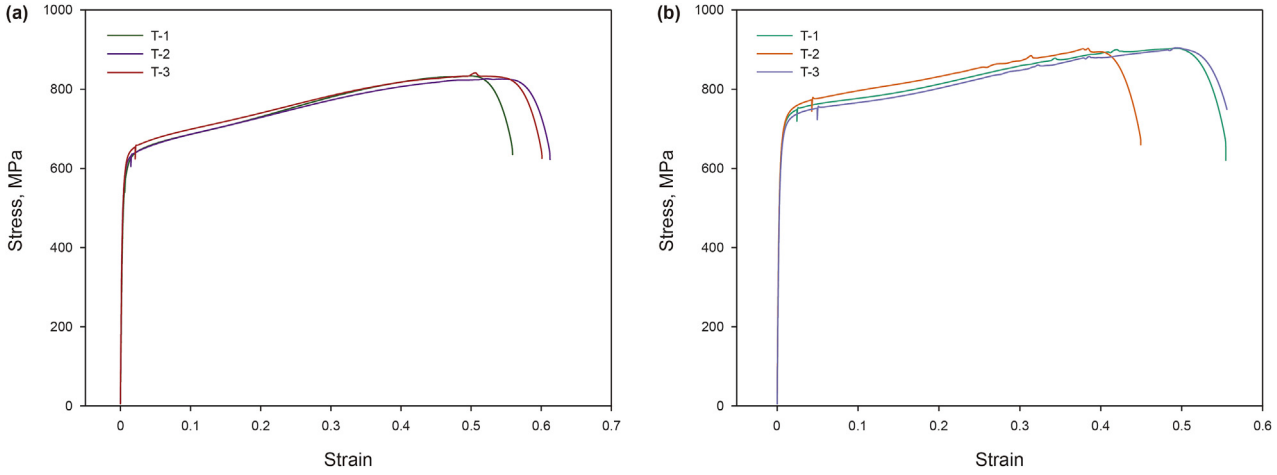

Fig. 10. Tensile test results: **(a)** 304 stainless steel, **(b)** 18Ni (T1, T2 and T3 are the specimen numbers).

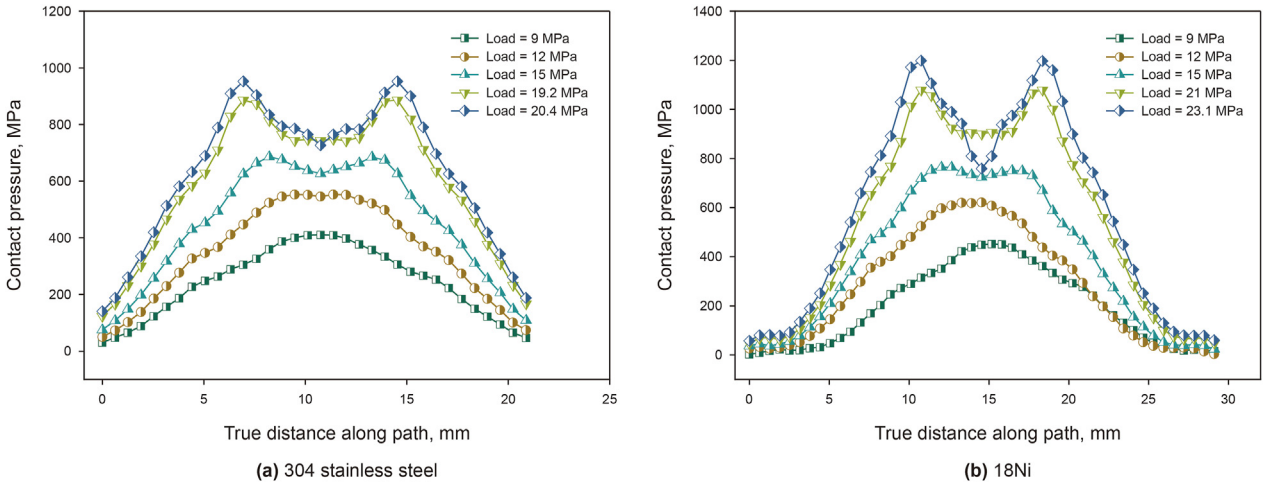

Fig. 11. The change in the monitoring curve of the contact pressure with the incremental steps of the load: **(a)** 304 stainless steel, **(b)** 18Ni.

preserving controller.

Displacement-time history curves of the maximum deformation monitoring points at different elastic moduli of the pressure controller under critical load conditions are obtained (Fig. 17). The load is gradually applied to the valve cover in step time. As the EM of the pressure-preserving controller increases, the displacement of the maximum deformation monitoring point decreases accordingly under the consistent load conditions. The larger the EM of the pressure-preserving controller is, the more obvious the decrease in the displacement of the maximum deformation monitoring point. Under the same load conditions, the EM increases from 160 GPa to 210 GPa, the displacement of the maximum deformation monitoring point of the pressure-preserving controller decreases from 0.60799 mm to 0.46565 mm, and the displacement decreases by 23.4%. Notably, the displacement of the maximum deformation monitoring point under the critical load is delayed to the maximum value with the increase in the EM of the pressure-preserving controller, and the final deformations are basically close, which are 0.60799, 0.60410, 0.60800, 0.61148, 0.61457, and 0.61116 mm, respectively.

3.2.4. *Influence of the PR on the UPB-Capability*

PR, also known as transverse deformation coefficient, is the ratio of the transverse strain to the longitudinal strain of the material. Since PR of metal materials does not vary widely, usually approximately 0.25–0.32 (Jia and Chen, 2016), the PRs in this paper are taken as 0.1, 0.2, 0.3, and 0.4, the EM is always taken as 200 GPa, and the model adopts the linear elastic model. The influence law of the PR on the UPB-Capability of the pressure-preserving controller is studied.

The change in the monitoring curve of the contact pressure with the incremental steps of the load under different PRs is shown in Fig. 18. The UPB-Capability of the pressure-preserving controller under different PRs is obtained, as shown in Fig. 19.

When PR is 0.1, 0.2, 0.3, and 0.4, the UPB-Capability of the pressure-preserving controller is 26.7, 27, 27.3, and 28.2 MPa, respectively. It can be seen that when the EM remains constant, with the increase in PR, the UPB-Capability of the pressure-preserving controller also increases. The PR increases by 300% from 0.1 to 0.4, and the UPB-Capability of the pressure-preserving controller increases by 5.62%. The calculation results show that the PR of the material has little effect on the UPB-Capability of the pressure-preserving controller.

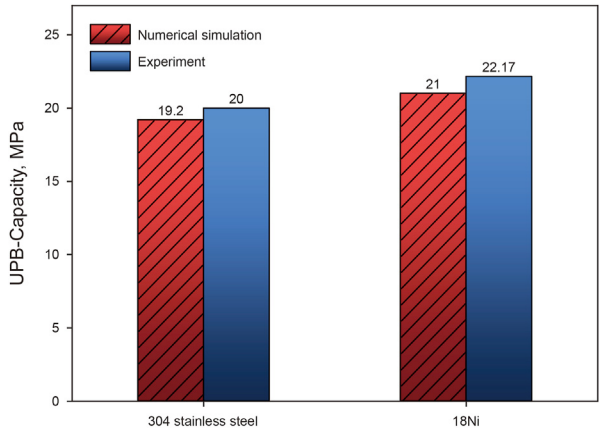

Fig. 12. Comparisons of simulation results and experimental results.

4. Discussion

The results show that the UPB-Capability of pressure-preserving controllers with different materials varies greatly. The EM of the material has a significant effect on the UPB-Capability of the pressure-preserving controller, whereas the YS and PR of the material have little effect. To further reveal the influence mechanism of material properties on the UPB-Capability of the pressure-preserving controller, the seal failure mechanism of the pressure-preserving controller is deeply analyzed, and the generalized model of the UPB-Capability of the pressure-preserving controller is established.

4.1. *Sealing failure mechanism of the pressure-preserving controller*

As seen in Fig. 17, the maximum deformation monitoring point displacement under critical load is delayed to the maximum value with the increase in the EM of the pressure-preserving controller, and the final deformation is basically close. This phenomenon indicates that the difference in the EM of the pressure-preserving controller eventually leads to different deformations of the maximum deformation monitoring point, which in turn affects the UPB-Capability of the pressure-preserving controller. There is a critical deformation of the maximum deformation monitoring point of the pressure-preserving controller, beyond which the

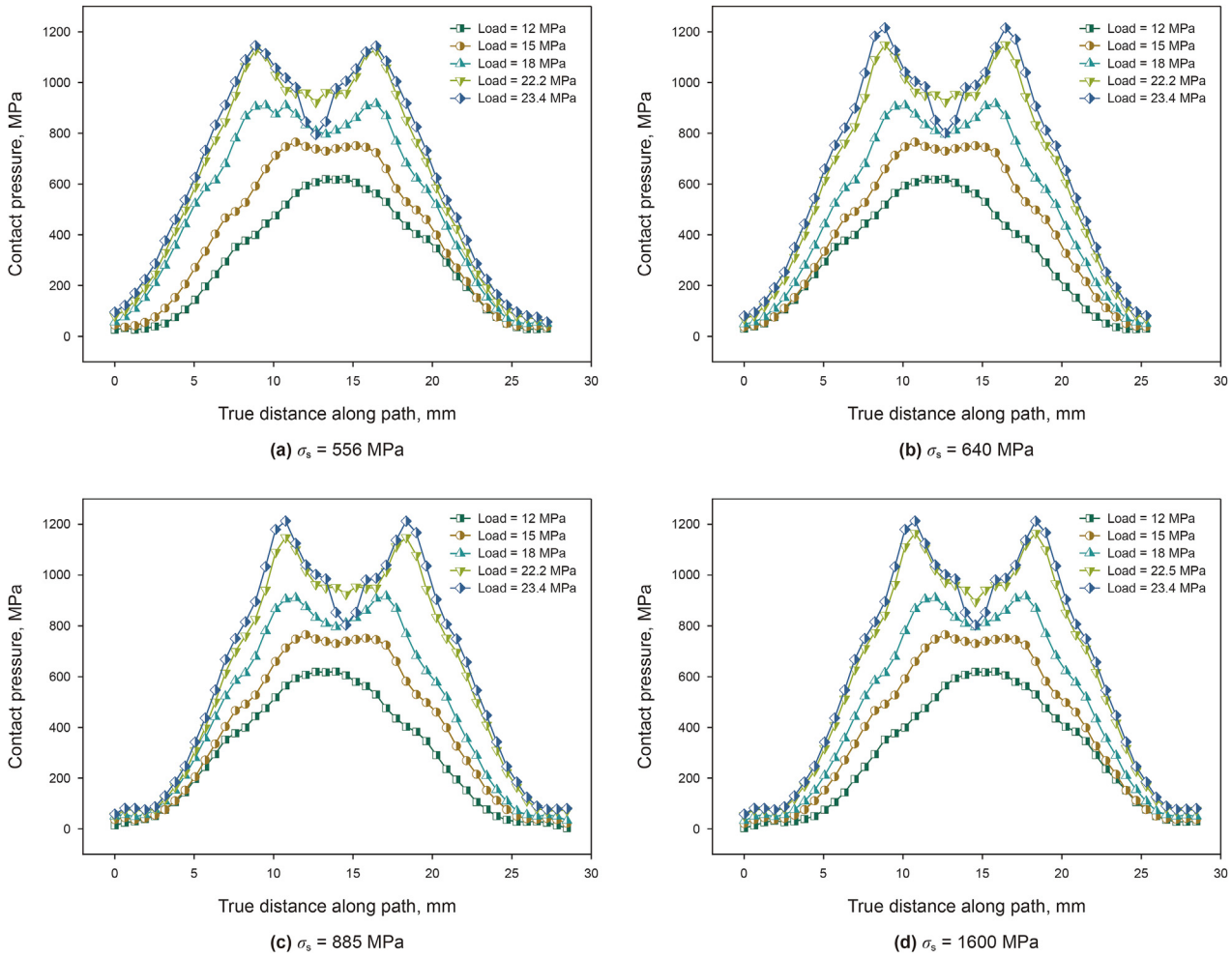

Fig. 13. The change in the monitoring curve of the contact pressure with the incremental steps of the load under different YSs.

pressure-preserving controller seal fails. The shrinkage of the valve covers short-axis edge before and after the test, as well as the smaller strain of the short-axis edge corresponding to the larger UPB-Capability of the pressure-preserving controller, also support this argument (Fig. 20). Taking the critical load of the A100 material pressure-preserving controller as an example, when the pressure is loaded to 17.75 MPa, the tensile strain in the BX direction of the pressure-preserving controller for the 304 stainless steel material is 1.92×10^{-3}, and the compressive strain in the BY direction is -2.30×10^{-3} (Fig. 8). The tensile strain in the BX direction of the pressure-preserving controller for the 35C material is 3.56×10^{-4}, and the compressive strain in the BY direction is -6.86×10^{-4}. The tensile strain in the BX direction of the pressure-preserving controller for the A100 material is 2.98×10^{-3}, and the compressive strain in the BY direction is -3.22×10^{-3}. The tensile strain in the BX direction of the pressure-preserving controller for the 18Ni material is 9.47×10^{-4}, and the compressive strain in the BY direction is -1.34×10^{-3}.

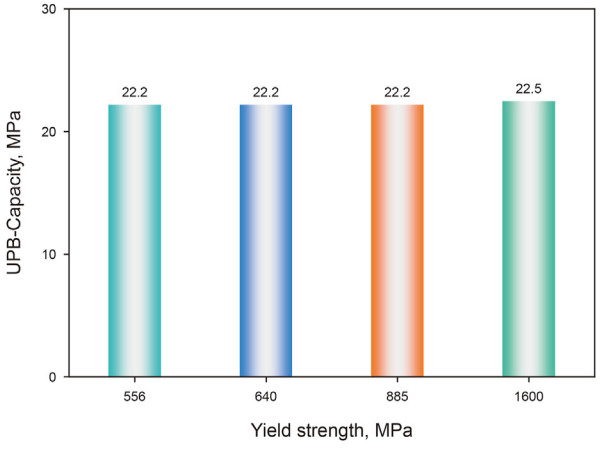

Fig. 14. The UPB-Capability of the pressure-preserving controller under different YSs.

The formation of a pressure-preserving controller compound seal designed according to the conical self-tensioning seal principle is a complex dynamic-static transformation process. The pressure-preserving controller mainly relies on the valve cover and valve seat to compress the O-ring at the beginning so that the contact pressure between the O-ring and the valve seat is greater than the medium pressure. Then, the initial seal is achieved, and the initial preload state has a small compression volume and extremely limited sealing capacity (Fig. 21(a)). With increasing differential pressure, the sealing gap is gradually compressed to the state in Fig. 21(b), the sealing capacity is improved, and the O-ring and valve seat sealing interface on the media leakage rate is gradually reduced. When the sealing gap is compressed to zero, the metal sealing surface begins to contact, and the pressure-preserving

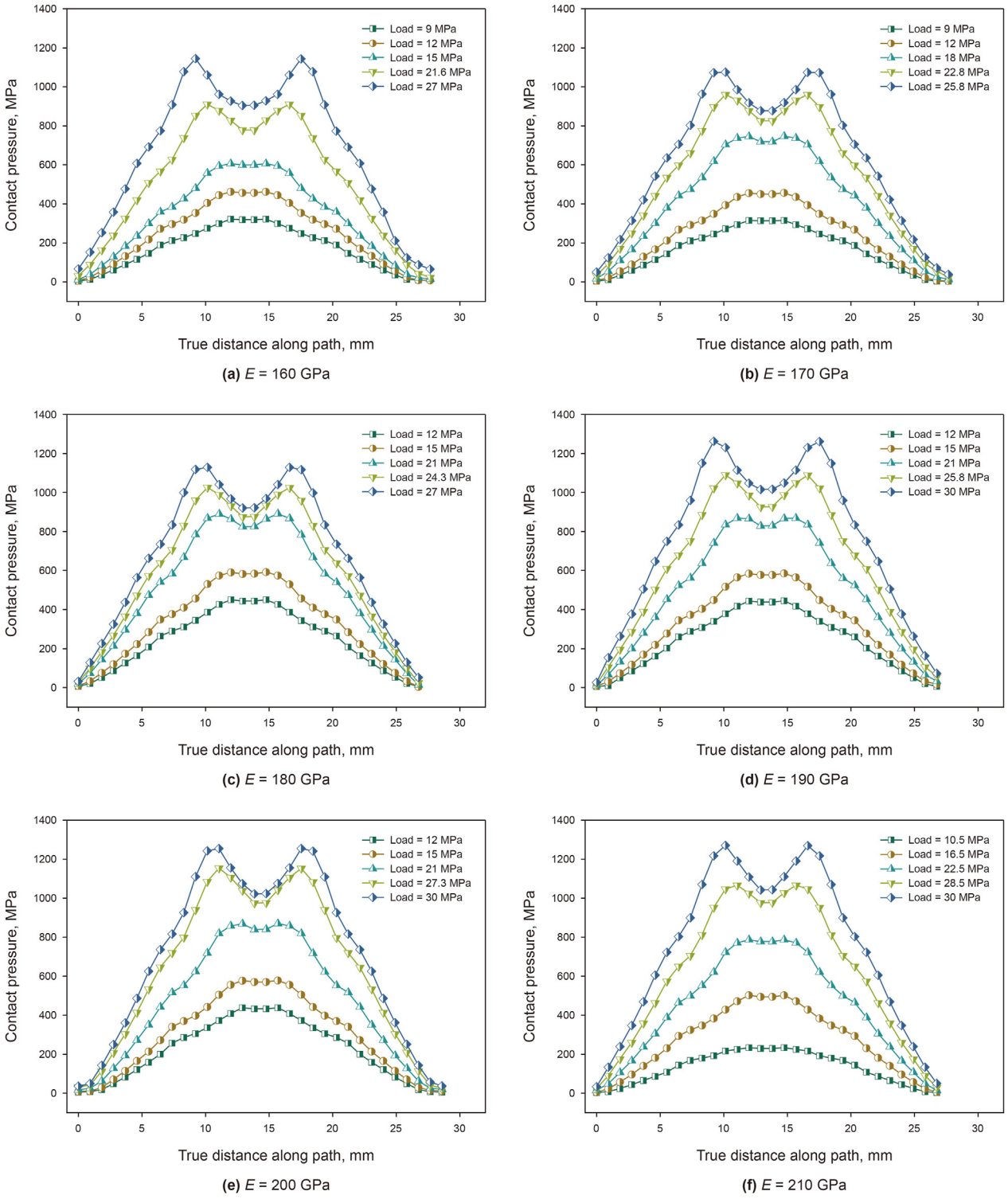

Fig. 15. The change in the monitoring curve of the contact pressure with the incremental steps of the load under different elastic moduli.

controller UPB-Capability reaches the maximum (Fig. 21(c)). When the differential pressure continues to increase, the deformation of the short shaft of the pressure-preserving controller exceeds the critical value, the O-ring is exposed, and the high-pressure medium acts directly on the O-ring (Fig. 21(d)). The O-ring is extruded and destroyed, and the pressure-preserving controller seal fails (Fig. 8(a)).

4.2. Generalized model of the pressure-preserving controller

The basic relations and equations of thin-shell theory are inherently complex, and the exact solution of the problem can be obtained only in some simple cases (Jawad, 1994). In contrast, the geometry and deformation of the pressure-preserving controller studied in this paper are extremely complex and must be

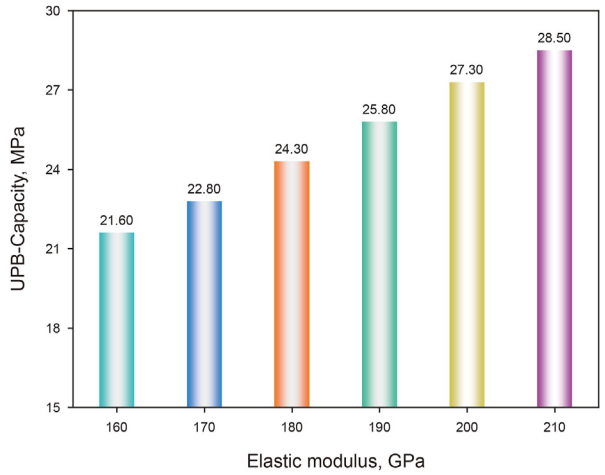

Fig. 16. The UPB-Capability of the pressure-preserving controller under different elastic moduli.

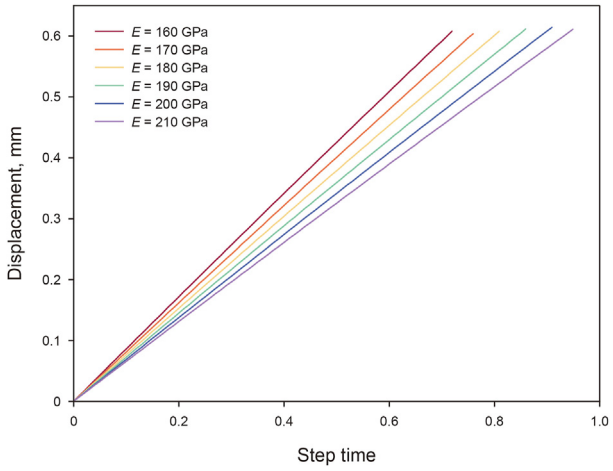

Fig. 17. Under the critical load condition, the displacement time-history curves of the pressure-preserving controller with different elastic moduli.

appropriately simplified to be solved. Therefore, in this paper, the pressure-preserving controller is simplified to a columnar thin shell (Fig. 22), and the generalized model of the pressure-preserving controller is established based on the basic assumptions of elastic mechanics and the Kirchhoff-Love hypothesis.

Based on the theory of column and shell with moments, a simplified model is established as shown in Fig. 23, assuming that the pressure-preserving controller is simply supported on four sides and introducing the dimensionless coordinate parameters $a/R = \alpha_1$, $b/R = \beta_1$, the boundary conditions are

$$\begin{array}{l}\text{When } \alpha = 0 \text{ and } \alpha = \alpha_1, v = w = M_1 = N_1 = 0\\ \text{When } \beta = 0 \text{ and } \beta = \beta_1, u = w = M_2 = N_2 = 0\end{array} \tag{1}$$

where a is the length of the column shell along the mother line, b is the length of the column shell along the perimeter, R is the radius in the cylindrical surface, u, v and w are the longitudinal, circumferential and normal displacements of the points in the face of the column shell, M_1, M_2 are the bending moments in the face of α and β, and N_1, N_2 are the tensile forces in the face of α and β, respectively.

The load conditions are $q_1 = 0$, $q_2 = 0$, $q_3 = -q_0$. The three equilibrium equations expressed by the displacement u, v and w are as follows (see Eq. (2)).

$$\begin{aligned}&\frac{\partial^2 u}{\partial^2 \alpha} + \frac{1-\mu}{2}\frac{\partial^2 u}{\partial^2 \beta} + \frac{1+\mu}{2}\frac{\partial^2 v}{\partial\alpha\partial\beta} = 0\\ &\frac{1+\mu}{2}\frac{\partial^2 u}{\partial\alpha\partial\beta} + \frac{\partial^2 v}{\partial\beta^2} + \frac{1-\mu}{2}\frac{\partial^2 v}{\partial\alpha^2} + \frac{\partial w}{\partial\beta} = 0\\ &\mu\frac{\partial u}{\partial\alpha} + \frac{\partial v}{\partial\beta} + C^2\nabla^2\nabla^2 w + w + \frac{(1-\mu^2)R^2}{Eh}q_0 = 0\end{aligned} \tag{2}$$

where $C^2 = \frac{h^2}{12R^2}$, h is the thickness of the shell. Introduce the function $\Phi(\alpha,\beta)$, and such that $\Phi(\alpha,\beta)$ satisfies

$$\begin{aligned}&\mu = \frac{\partial^3\Phi}{\partial\alpha\partial\beta^2} - \mu\frac{\partial^3\Phi}{\partial\alpha^3}\\ &v = -(2+\mu)\frac{\partial^3\Phi}{\partial\alpha^2\partial\beta} - \mu\frac{\partial^3\Phi}{\partial\beta^3}\\ &w = \nabla^2\nabla^2\Phi\end{aligned} \tag{3}$$

Substituting Eq. (3) into Eq. (2), the first two equations are naturally satisfied, and the third equation is reduced to an eighth-order partial differential equation:

$$\nabla^2\nabla^2\nabla^2\nabla^2\Phi + \frac{(1-\mu^2)}{C^2}\frac{\partial^4\Phi}{\partial\alpha^4} = -\frac{R^4}{D}q_0 \tag{4}$$

where $D = \frac{Eh^3}{12(1-\mu^2)}$, D is the flexural stiffness of the shell. Selecting double trigonometric series:

$$\Phi(\alpha,\beta) = \sum_{m=1}^{\infty}\sum_{n=1}^{\infty} A_{mn}\sin\frac{m\pi\alpha}{\alpha_1}\sin\frac{n\pi\beta}{\beta_1} \tag{5}$$

where A_{mn} is the undetermined coefficient,

$$\begin{aligned}&\text{When } \alpha = 0 \text{ and } \alpha = \alpha_1, \Phi = \frac{\partial^2\Phi}{\partial\alpha^2} = \frac{\partial^4\Phi}{\partial\alpha^4} = \frac{\partial^6\Phi}{\partial\alpha^6} = 0\\ &\text{When } \beta = 0 \text{ and } \beta = \beta_1, \Phi = \frac{\partial^2\Phi}{\partial\beta^2} = \frac{\partial^4\Phi}{\partial\beta^4} = \frac{\partial^6\Phi}{\partial\beta^6} = 0\end{aligned} \tag{6}$$

Obviously, Eq. (5) has satisfied the boundary conditions. Substituting equation Eq. (5) into equation Eq. (4) gives

$$\begin{aligned}&\sum_{m=1}^{\infty}\sum_{n=1}^{\infty} A_{mn}\left\{\left[\left(\frac{m\pi}{\alpha_1}\right)^2 + \left(\frac{n\pi}{\beta_1}\right)^2\right]^4 + \frac{(1-\mu^2)}{C^2}\left(\frac{m\pi}{\alpha_1}\right)^4\right\}\sin\frac{m\pi\alpha}{\alpha_1}\sin\frac{m\pi\beta}{\beta_1}\\ &= -\frac{R^4}{D}q_0\end{aligned} \tag{7}$$

Let $B_{mn} = \frac{D}{R^4}A_{mn}\left\{\left[\left(\frac{m\pi}{\alpha_1}\right)^2 + \left(\frac{n\pi}{\beta_1}\right)^2\right]^4 + \frac{(1-\mu^2)}{C^2}\left(\frac{m\pi}{\alpha_1}\right)^4\right\}$, Substituting into Eq. (7), we get

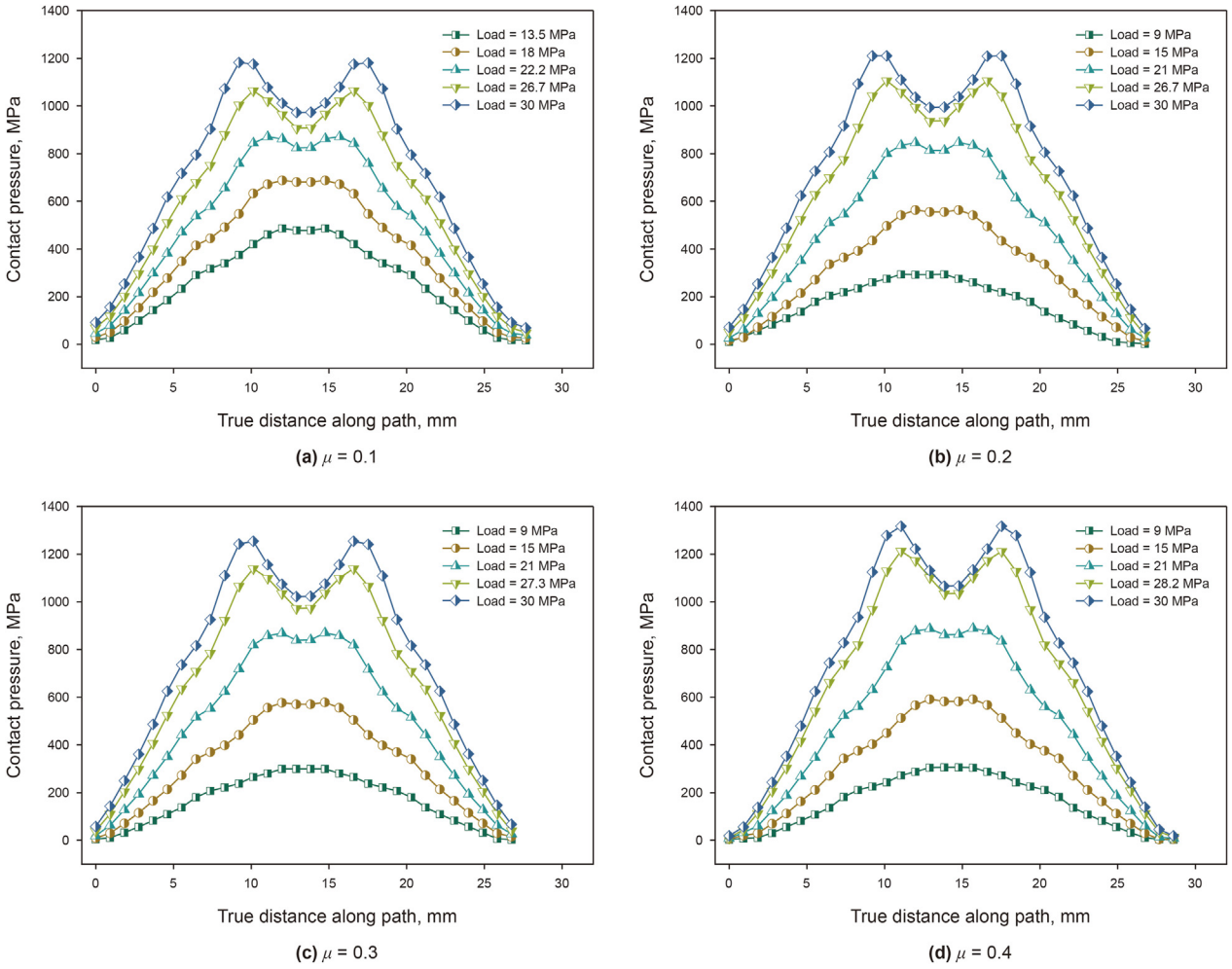

Fig. 18. The change in the monitoring curve of the contact pressure with the incremental steps of the load under different PRs.

$$\sum_{m=1}^{\infty}\sum_{n=1}^{\infty} B_{mn}\sin\frac{m\pi\alpha}{\alpha_1}\sin\frac{m\pi\beta}{\beta_1} = -q_0 \tag{8}$$

Multiply the two sides of the Eq. (8) by $\sin\frac{i\pi\alpha}{\alpha_1}\mathrm{d}\alpha$ and $\sin\frac{i\pi\beta}{\beta_1}\mathrm{d}\beta$ (where i is any positive integer), respectively, and integrate to obtain

$$B_{mn} = \frac{4}{\alpha_1\beta_1}\int_0^{\alpha_1}\int_0^{\beta_1} -q_0\sin\frac{m\pi\alpha}{\alpha_1}\sin\frac{n\pi\beta}{\beta_1}\mathrm{d}\alpha\mathrm{d}\beta \tag{9}$$

$$A_{mn} = \frac{4R^4}{\alpha_1\beta_1 D}\frac{\int_0^{\alpha_1}\int_0^{\beta_1} -q_0\sin\frac{m\pi\alpha}{\alpha_1}\sin\frac{n\pi\beta}{\beta_1}\mathrm{d}\alpha\mathrm{d}\beta}{\left\{\left[\left(\frac{m\pi}{\alpha_1}\right)^2+\left(\frac{n\pi}{\beta_1}\right)^2\right]^4+\frac{(1-\mu^2)}{C^2}\left(\frac{m\pi}{\alpha_1}\right)^4\right\}} = -\frac{16R^4q_0}{Dmn\pi^2}\frac{1}{\left\{\left[\left(\frac{m\pi}{\alpha_1}\right)^2+\left(\frac{n\pi}{\beta_1}\right)^2\right]^4+\frac{1-\mu^2}{C^2}\left(\frac{m\pi}{\alpha_1}\right)^4\right\}} \quad (m, n = 1, 3, 5, \cdots) \tag{10}$$

Substituting A_{mn} into Eq. (5), the function $\Phi(\alpha,\beta)$ is obtained as

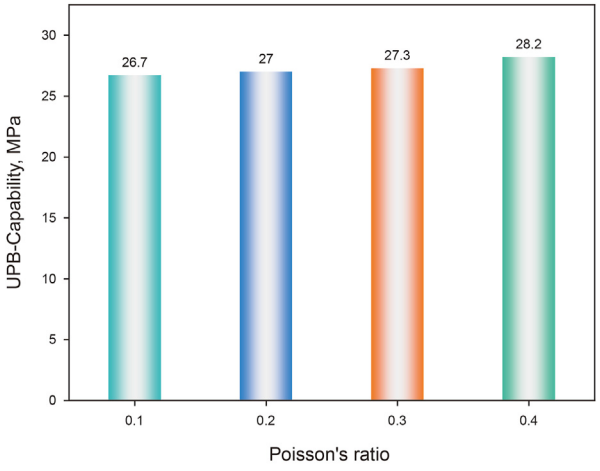

Fig. 19. The UPB-Capability of the pressure-preserving controller under different PRs.

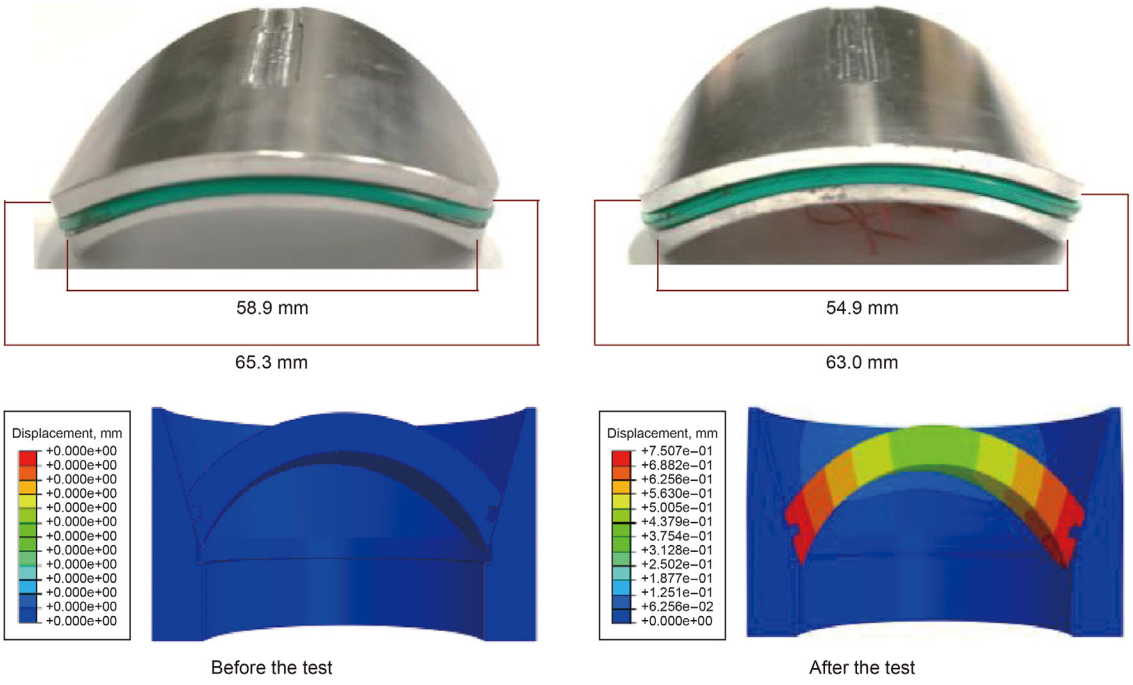

Fig. 20. The pressure-preserving controller valve cover retracted.

$$\Phi(\alpha,\beta)=\frac{4R^4}{\alpha_1\beta_1 D}\sum_{m=1}^{\infty}\sum_{n=1}^{\infty}\frac{\int_0^{\alpha_1}\int_0^{\beta_1} q_0\sin\frac{m\pi\alpha}{\alpha_1}\sin\frac{n\pi\beta}{\beta_1}\mathrm{d}\alpha\mathrm{d}\beta}{\left\{\left[\left(\frac{m\pi}{\alpha_1}\right)^2+\left(\frac{n\pi}{\beta_1}\right)^2\right]^4+\frac{(1-\mu^2)}{C^2}\left(\frac{m\pi}{\alpha_1}\right)^4\right\}}\sin\frac{m\pi\alpha}{\alpha_1}\sin\frac{n\pi\beta}{\beta_1}$$
$$=-\frac{16R^4q_0}{Dmn\pi^2}\frac{\sin\frac{m\pi\alpha}{\alpha_1}\sin\frac{n\pi\beta}{\beta_1}}{\left\{\left[\left(\frac{m\pi}{\alpha_1}\right)^2+\left(\frac{n\pi}{\beta_1}\right)^2\right]^4+\frac{1-\mu^2}{C^2}\left(\frac{m\pi}{\alpha_1}\right)^4\right\}}\quad(m,\ n=1,\ 3,\ 5,\ \cdots)\tag{11}$$

Substitute Eq. (11) into Eq. (3) and then get

$$\mathrm{u}=-\frac{16\nu}{\pi^3}\frac{Rq_0a}{Eh}\sum_{m}^{\infty}\sum_{n}^{\infty}\frac{\mu m^2-\lambda^2n^2}{n\left[\left(m^2+\lambda^2n^2\right)^4+\nu m^4\right]}\cos\frac{m\pi a}{\alpha_1}\sin\frac{n\pi\beta}{\beta_1}$$
$$\nu=-\frac{16\lambda\nu}{\pi^3}\frac{Rq_0a}{Eh}-\sum_{m}^{\infty}\sum_{n}^{\infty}\frac{\lambda^2n^2+(2+\mu)m^2}{m\left[\left(m^2+\lambda^2n^2\right)^4+\nu m^4\right]}\sin\frac{m\pi\alpha}{\alpha_1}\cos\frac{n\pi\beta}{\beta_1}\tag{12}$$
$$w=\frac{192q_0a^4(1-\mu^2)}{\pi^6Eh^3}(w_k-w_0)$$

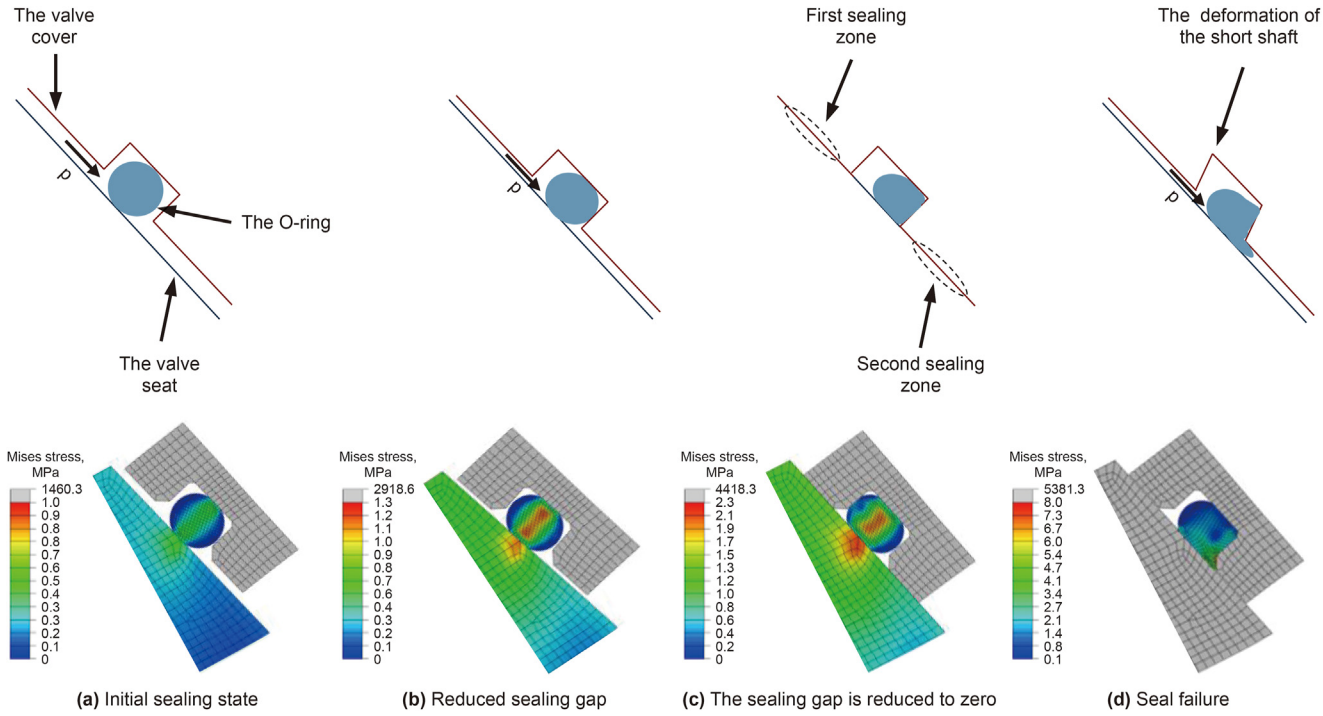

Fig. 21. Diagram of seal failure process.

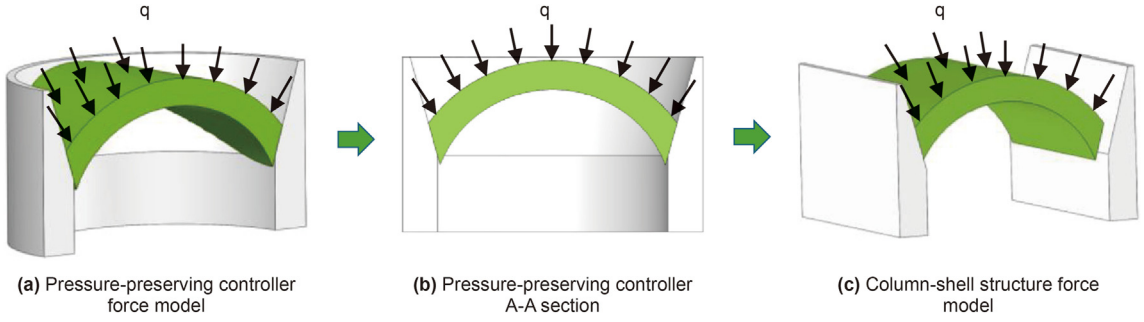

Fig. 22. The pressure-preserving controller force analysis simplified ideas.

where $w_k = \nu \sum_{m}^{\infty} \sum_{n}^{\infty} \frac{m^3 \sin\frac{m\pi\alpha}{\alpha_1} \sin\frac{n\pi\beta}{\beta_1}}{n\left(m^2+\lambda^2 n^2\right)^2\left[\left(m^2+\lambda^2 n^2\right)^4+\nu m^4\right]}$, $w_0 = \sum_{m}^{\infty} \sum_{n}^{\infty} \frac{\sin\frac{m\pi\alpha}{\alpha_1} \sin\frac{n\pi\beta}{\beta_1}}{mn\left(m^2+\lambda^2 n^2\right)^2}$, and $\lambda = \frac{\alpha_1}{\beta_1} = \frac{a}{b} = 1.04$, $\nu = \frac{1-\mu^2}{C^2}\frac{\alpha_1^4}{\pi^4} = \frac{12\left(1-\mu^2\right)}{\pi^4}\frac{a^4}{R^2h^2} = \frac{3807.4\left(1-\mu^2\right)}{h^2}$.

When only the first term of the series is taken, there is

$$w = \frac{-192q_0a^4\left(1+\lambda^2\right)^4\left(1-\mu^2\right)\sin\frac{\pi\alpha}{\alpha_1}\sin\frac{\pi\beta}{\beta_1}}{\pi^6Eh^3\left(1+\lambda^2\right)^2\left[\left(1+\lambda^2\right)^4+\nu\right]} = \frac{-3.37\times10^7q_0\sin\frac{\pi\alpha}{\alpha_1}\sin\frac{\pi\beta}{\beta_1}}{Eh\left[\frac{18.78h^2}{\left(1-\mu^2\right)}+3807.4\right]} \tag{13}$$

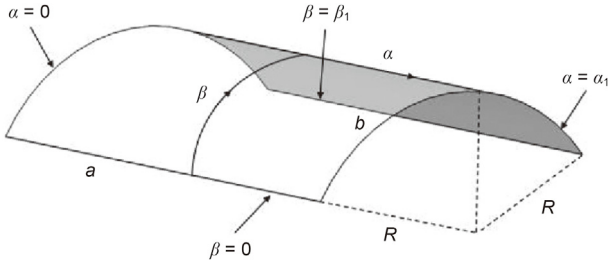

Fig. 23. Simplified model of the pressure-preserving controller.

As stated above, the seal failure of the pressure-preserving controller is caused by the large deformation of the short shaft of the pressure-preserving controller, so as long as the deformation of the short shaft of the pressure-preserving controller is reduced, the UPB-Capability of the pressure-preserving controller can be increased. From Eq. (13), we can see that w is negatively correlated with h and μ and inversely proportional to E, which explains why with the increase in EM and PR, the UPB-Capability of the pressure-preserving controller increases, and EM has a significant effect on the UPB-Capability of the pressure-preserving controller, whereas PR has little effect. Although there is a positive effect on improving

the UPB-Capability of pressure-preserving controllers by selecting materials with higher EM, the increase in UPB-Capability comes at the expense of sealing performance because materials with lower EM can effectively improve the contact properties of the sealing interface, as mentioned by Li et al. (2022b). Therefore, in practical engineering applications, when the UPB-Capability of a pressure-preserving controller cannot meet the engineering requirements, one must select materials with a high EM; when the UPB-Capability of a pressure-preserving controller meets the engineering requirements, one must select materials with a low EM. At the same time, we propose that the future optimization direction of pressure-preserving controllers can be carried out using the following steps: first, choosing materials with high EM; second, thickening the valve cover as much as the assembly space allows; and third, limiting the deformation of the short shaft edge by increasing the limiting steps.

Although this paper reveals the influence mechanism of material mechanical parameters on the UPB-Capability of the pressure-preserving controller from another angle by establishing the generalized model of the pressure-preserving controller, it should be pointed out that due to the gap between the actual structure and the theoretical model, the establishment of a more realistic theoretical model will be the direction of improvement in the future. The significance of this paper lies in the fact that the numerical simulation shows intuitively the influence mechanism of the material mechanical parameters on the UPB-Capability of the pressure-preserving controller, which is difficult to be revealed in physical experiments, and the generalized model established also provides a theoretical basis for the further optimization of the structure of the pressure-preserving controller.

5. Conclusions

To achieve a good understanding of the influence of material mechanical properties on the UPB-Capability of pressure-preserving controllers, laboratory tests and numerical simulations were conducted. An in-depth analysis of the sealing failure mechanisms of pressure-preserving controllers has been carried out, revealing the influence mechanism of material properties on the UPB capabilities of pressure-preserving controllers. The conclusions are as follows.

(1) The EM of the material has a significant effect on the UPB-Capability of a pressure-preserving controller, whereas the YS and PR of the material have little effect. With an increase in the EM, the UPB-Capability of a pressure-preserving controller increases almost linearly.
(2) There is a critical value for the deformation of the short shaft of a pressure-preserving controller, and seal failure is caused by the large deformation of its short shaft. Materials with higher EM have positive significance in reducing the short shaft deformation of a pressure-preserving controller and improving its UPB-Capability.
(3) In practical engineering applications, when the UPB-Capability of a pressure-preserving controller cannot meet the engineering requirements, one must choose materials with high EM; when the UPB-Capability of a pressure-preserving controller meets the engineering requirements, one must choose materials with low EM.
(4) The future optimization directions of pressure-preserving controllers can be carried out using the following steps: first, choosing materials with high EM; second, thickening the valve cover as much as the assembly space allows; and third, limiting the deformation of the short shaft edge by increasing the limiting steps.

CRediT authorship contribution statement

Xiao-Jun Shi: Writing – review & editing, Writing – original draft, Software, Formal analysis, Data curation, Conceptualization. **He-Ping Xie:** Writing – review & editing, Supervision, Funding acquisition. **Cong Li:** Validation, Supervision, Methodology, Formal analysis. **Gui-Kang Liu:** Visualization, Software, Investigation. **Zi-Jie Wei:** Writing – review & editing, Investigation, Data curation. **Tian-Yu Wang:** Software, Investigation. **Ju Li:** Investigation, Formal analysis. **Qiu-Yue Li:** Writing – review & editing, Resources, Investigation.

Declaration of competing interest

The authors declare that they have no known competing financial interests or personal relationships that could have appeared to influence the work reported in this paper.

Acknowledgements

This study was financially supported by the National Natural Science Foundation of China (Grant Nos. 52225403, 52304146, 51827901) and Sichuan Science and Technology Program (2023NSFSC0919).

References

Abegg, F., Hohnberg, H.J., Pape, T., et al., 2008. Development and application of pressure-core-sampling systems for the investigation of gas- and gas-hydrate-bearing sediments. Deep-Sea Res. Part I Oceanogr. Res. Pap. 55 (11), 1590–1599. https://doi.org/10.1016/j.dsr.2008.06.006.

Belforte, G., Conte, M., Manuello Bertetto, A., et al., 2018. Indirect contact pressure evaluation on pneumatic rod seals. Tribol. Int. 118, 240–245. https://doi.org/10.1016/j.triboint.2017.10.002.

Bhakta, T., Avseth, P., Landrø, M., 2016. Sensitivity analysis of effective fluid and rock bulk modulus due to changes in pore pressure, temperature and saturation. J. Appl. Geophys. 135, 77–89. https://doi.org/10.1016/j.jappgeo.2016.09.012.

Burger, J., Gupta, D., Jacobs, P., et al., 2003. Overview on Hydrate Coring, Handling and Analysis. United States. https://doi.org/10.2172/908303.

Chen, J.W., Fan, W., Bingham, B., 2013. A long gravity-piston corer developed for seafloor gas hydrate coring utilizing an in situ pressure-retained method. Energies 6 (7), 3353–3372. https://doi.org/10.3390/en6073353.

Chen, J.W., Ge, H., Fu, M.R., 2017. Structure modify of high-pressure chamber in pressure-retaining sampler for deep-sea sediment. J. Inst. Eng.: Series C 98 (5), 619–624. https://doi.org/10.1007/s40032-017-0360-3.

Gao, M.Z., Yang, B.G., Xie, J., et al., 2022. The mechanism of microwave rock breaking and its potential application to rock-breaking technology in drilling. Petrol. Sci. 19 (3), 1110–1124. https://doi.org/10.1016/j.petsci.2021.12.031.

Gao, M.Z., Chen, L., Fan, D., et al., 2021a. Principle and technology of coring with in-situ pressure and gas maintaining in deep coal mine. J. China Coal Soc. 46 (3), 885–897. https://doi.org/10.13225/j.cnki.jccs.YT21.0297 (in Chinese).

Gao, M.Z., Xie, J., Gao, Y.N., et al., 2021b. Mechanical behavior of coal under different mining rates: a case study from laboratory experiments to field testing. Int. J. Min. Sci. Technol. 31 (5), 825–841. https://doi.org/10.1016/j.ijmst.2021.06.007.

Garel, M., Bonin, P., Martini, S., et al., 2019. Pressure-retaining sampler and high-pressure systems to study deep-sea microbes under in situ conditions. Front. Microbiol. 10, 1–13. https://doi.org/10.3389/fmicb.2019.00453.

Guo, D., Xie, H.P., Chen, L., et al., 2023. In-situ pressure-preserved coring for deep exploration: insight into the rotation behavior of the valve cover of a pressure controller. Petrol. Sci. 20 (4), 2386–2398. https://doi.org/10.1016/j.petsci.2023.02.020.

Guo, J., Wang, Y., Wang, W., et al., 2022. Pressure-retaining sampler for sediment including overlying water based on heavy duty ROV-Jellyfish. Appl. Ocean Res. 128, 103354. https://doi.org/10.1016/j.apor.2022.103354.

He, S.D., Qiu, S.W., Tang, W.B., et al., 2023. A novel submersible-mounted sediment pressure-retaining sampler at full ocean depth. Front. Mar. Sci. 10, 1154269. https://doi.org/10.3389/fmars.2023.1154269.

He, S.T., Zhao, Y., Yuan, H., 2011. Ultimate strength of cylindrical shell with circumferential crack damage considering crack extension. ShipBuild. China. 52 (4), 23–37 (in Chinese).

He, Z.Q., Chen, L., Lu, T., et al., 2019. The optimization of pressure controller for deep earth drilling. Therm. Sci. 23, 123. https://doi.org/10.2298/TSCI180612123H, 123.

Hohnberg, H.J., Amann, H., Abegg, F., et al.. Pressurized coring of near-surface gas-hydrate sediments on hydrate ridge: the multiple autoclave corer, and first results from pressure-core X-ray CT Scan. https://api.semanticscholar.org/

CorpusID:231099297.
Hu, Y.Q., Xie, J., Xue, S.N., et al., 2022. Research and application of thermal insulation effect of natural gas hydrate freezing corer based on the wireline-coring principle. Petrol. Sci. 19 (3), 1291–1304. https://doi.org/10.1016/j.petsci.2021.11.019.
Huang, W., Li, J.N., Liu, Z.Q., et al., 2023. Study of a low-disturbance pressure-preserving corer and its coring performance in deep coal mining conditions. Int. J. Min. Sci. Technol. 33 (11), 1397–1410. https://doi.org/10.1016/j.ijmst.2023.07.003.
Jackson, K., Witte, U., Chalmers, S., et al., 2017. A system for retrieval and incubation of benthic sediment cores at in situ ambient pressure and under controlled or manipulated environmental conditions. J. Atmos. Ocean. Technol. 34, 983–1000. https://doi.org/10.1175/JTECH-D-16-0248.1.
Jackson, R.L., Green, I., 2005. A finite element study of elasto-plastic hemispherical contact against a rigid flat. J. Tribol. 127 (2), 343–354. https://doi.org/10.1115/1.1866166.
Jawad, M.H., 1994. Theory and Design of Plate and Shell Structures.
Jia, C.C., Chen, F.R., 2016. Mechanical parameters of materials on the stress of ultrasonic impact treatment after welding Finite element simulation of the effect of strain. Trans. China Weld. Inst. 37 (10), 105–108+135 (in Chinese).
Kawasaki, M., Umezu, S., Yasuda, M., 2006. Pressure temperature core sampler (PTCS). J. Jpn. Assoc. Pet. Technol. 71, 139–147. https://doi.org/10.3720/japt.71.139.
Kong, L.W., Xie, H.P., Li, C.B., 2023. Coupled microplane and micromechanics model for describing the damage and plasticity evolution of quasi-brittle material. Int. J. Plast. 162, 103549. https://doi.org/10.1016/j.ijplas.2023.103549.
Li, C., Pei, J.L., Wu, N.H., et al., 2022a. Rotational failure analysis of spherical-cylindrical shell pressure controllers related to gas hydrate drilling investigations. Petrol. Sci. 19 (2), 789–799.
Li, C., Xie, H.P., Gao, M.Z., et al., 2021. Novel designs of pressure controllers to enhance the upper pressure limit for gas-hydrate-bearing sediment sampling. Energy 227, 120405. https://doi.org/10.1016/j.petsci.2022.02.005.
Li, C.B., Yang, D.C., Xie, H.P., et al., 2023. Size effect of fracture characteristics for anisotropic quasi-brittle geomaterials. Int. J. Min. Sci. Technol. 33 (2), 201–213. https://doi.org/10.1016/j.ijmst.2022.11.004.
Li, J.N., Wang, J., Hu, Y.Q., et al., 2022b. Contact performance analysis of pressure controller's sealing interface in deep in-situ pressure-preserving coring system. Petrol. Sci. 19 (3), 1334–1346. https://doi.org/10.1016/j.petsci.2021.11.022.
Liang, W.W., Li, C., Liu, G.K., et al., 2023. Pressure-bearing characteristics of pressure-preserved controllers under deep in-situ temperature and pressure conditions. Coal Geol. Explor. 51 (8), 68–78. https://doi.org/10.12363/issn.1001-1986.23.07.0407 (in Chinese).
Liu, G.K., Gao, M.Z., Yang, Z.W., et al., 2020. The innovative design of deep in situ pressure retained coring based on magnetic field trigger controller. Adv. Civ. Eng. 2020, 1–15. https://doi.org/10.1155/2020/8873628.
Ma, D.D., Wu, Y., Yin, J.D., et al., 2023. Effect of initial pore pressure on the hydraulic fracturing of tight sandstone: an experimental study. Geomech. Geophys. Geo-Energy Geo-Resour. 9 (1), 15. https://doi.org/10.1007/s40948-023-00547-x.
Peng, C., Fischer, F.J., Schmitz, K., et al., 2021. Comparative analysis of leakage calculations for metallic seals of ball-seat valves using the multi-asperity model and the magnification-based model. Tribol. Int. 163, 107130. https://doi.org/10.1016/J.TRIBOINT.2021.107130.
Pettigrew, T.L., 1992. Design and operation of a wireline presure core sampler (PCS). Ocean Drilling Program Technical Notes. https://doi.org/10.2973/ODP.TN.17.1992.
Qin, H.W., Cai, Z., Hu, H.M., et al., 2016. Numerical analysis of gravity coring using coupled eulerian-Lagrangian method and a new corer. Mar. Georesour. Geotechnol. 34 (5), 403–408. https://doi.org/10.1080/1064119X.2014.958880.
Qin, H.W., Gu, L.Y., Li, S.L., et al., 2005. Pressure tight piston corer—a new approach on gas hydrate investigation. China Ocean Eng. 19, 121–128. https://doi.org/10.3321/j.issn:0890-5487.2005.01.011.
Ren, J.X., Yun, M.C., Zhang, K., 2021. Study on mechanical properties of triaxial unloading of granite under pore pressure. IOP Conf. Ser. Earth Environ. Sci. 643 (1), 012020. https://doi.org/10.1088/1755-1315/643/1/012020.
Shen, S., Li, Y.H., Sun, X., et al., 2022. Mechanical properties of methane hydrate-bearing sandy sediments under various temperatures and pore pressures. J. Petrol. Sci. Eng. 208, 109474. https://doi.org/10.1016/j.petrol.2021.109474.
Shi, X.J., Li, J.N., Li, C., et al., 2023. Design and strength analysis of the passive thermal insulation structure of a deep rock in-situ thermal insulation coring system. Therm. Sci. 27, 623–630. https://doi.org/10.2298/TSCI2301623S.
Sukumar, T., Subramanian, M., Subramaniyan, S., et al., 2015. Design and optimization of lip seal for air braking system. SAE Tech. Pap. https://doi.org/10.4271/2015-26-0215.
Sun, B.J., Li, X.F., Wang, Z.Y., et al., 2023. Laboratory investigation of the effect of the pore pressure on argillaceous siltstone permeability. Eng. Geol. 317, 107067. https://doi.org/10.1016/j.enggeo.2023.107067.
Wang, J.L., Sun, Y., Qian, D.L., et al., 2022. Scheme design and performance analysis of thin-walled pressure-retaining coring tools for seafloor drills in the deep-sea operating environment. J. Petrol. Sci. Eng. 208, 109790. https://doi.org/10.1016/j.petrol.2021.109790.
Wang, W., Liu, D., Jin, Y., et al., 2021. Simulation analysis of sample temperature of the whole deep-sea macro biosampler recovery process. Ocean Engineering Equipment and Technology 8 (1), 64–69 (in Chinese).
Wei, K., He, B.L., Yang, Y.J., 2015. Effect of wheel material properties on wheel-rail contact stress based on ANSYS. Surf. Technol. 44 (5), 125–128. https://doi.org/10.16490/j.cnki.issn.1001-3660.2015.05.023.
Wu, D.Y., Peng, J.M., Sun, M.Z., et al., 2016. Experimental study on a pressure-coring technology based on a freeze-core valve for marine hydrate-bearing sediment sampling. J. Nat. Gas Sci. Eng. 33, 135–142. https://doi.org/10.1016/j.jngse.2016.05.023.
Wu, N.H., Xie, H.P., Chen, L., et al., 2020. Sealing form and failure mechanism of deep in situ rock core pressure-maintaining controller. Geofluids 2020, 1–15. https://doi.org/10.1155/2020/8892720.
Wu, S.J., Yang, C.J., Chen, Y., et al., 2010. A study of the sealing performance of a new high-pressure cone valve for deep-sea gas-tight water samplers. J. Pressure Vessel Technol. 132 (4). https://doi.org/10.1115/1.4001204.
Xie, H.P., Liu, T., Gao, M.Z., et al., 2021a. Research on in-situ condition preserved coring and testing systems. Petrol. Sci. 18 (6), 1840–1859. https://doi.org/10.1016/j.petsci.2021.11.003.
Xie, H.P., Gao, M.Z., Zhang, R., et al., 2020. Study on concept and progress of in situ fidelity coring of deep rocks. Chin. J. Rock Mech. Eng. 39 (5), 865–876. https://doi.org/10.13722/j.cnki.jrme.2020.0138 (in Chinese).
Xie, H.P., Gao, M.Z., Zhang, R., et al., 2019. Study on the mechanical properties and mechanical response of coal mining at 1000 m or deeper. Rock Mech. Rock Eng. 52 (5), 1475–1490. https://doi.org/10.1007/s00603-018-1509-y.
Xie, H.P., Hu, Y.Q., Gao, M.Z., et al., 2023a. Research progress and application of deep in-situ condition preserved coring and testing. Int. J. Min. Sci. Technol. 33 (11), 1319–1337. https://doi.org/10.1016/j.ijmst.2023.06.007.
Xie, H.P., Li, C., He, Z.Q., et al., 2021b. Experimental study on rock mechanical behavior retaining the in situ geological conditions at different depths. Int. J. Rock Mech. Min. Sci. 138, 104548. https://doi.org/10.1016/j.ijrmms.2020.104548.
Xie, H.P., Lu, J., Li, C., et al., 2022. Experimental study on the mechanical and failure behaviors of deep rock subjected to true triaxial stress: a review. Int. J. Min. Sci. Technol. 32 (5), 915–950. https://doi.org/10.1016/j.ijmst.2022.05.006.
Xie, L.X., Li, L., Jiang, G.Z., et al., 2015. Numerical study of the contact pressure of window-type vane seals: Part I. Seal. Technol. 3, 7–12. https://doi.org/10.1016/S1350-4789(15)30051-9.
Xie, Y., Hou, M.Z., Liu, H.J., et al., 2023b. Anisotropic time-dependent behaviors of shale under direct shearing and associated empirical creep models. J. Rock Mech. Geotech. Eng. https://doi.org/10.1016/j.jrmge.2023.05.001.
Zhang, B.W., Liu, J.P., Xu, Q., 2019. Influence of mechanical properties of materials on the ultimate strength of spherical pressure structure. Ship Eng. 41 (12), 113–118 (in Chinese).
Zhang, J.F., Cui, W.C., 2003. Comparison of ultimate strength analysis of three types of ship structures. J. Ship Mech. 7 (4), 57–64 (in Chinese).
Zhang, S.J., 2018. Analysis on the Effects of Material and Structural Defects on the Property of Deep-Sea Manned Spherical Hull. Jiangsu University of Science and Technology. Thesis. Jiangsu, China, 1–10 (in Chinese).
Zhao, X.L., Huang, B.X., Chen, B., et al., 2022. Experimental investigation of the effect of evenly distributed pore pressure on rock damage. Lithosphere 2021. https://doi.org/10.2113/2022/1759146.
Zhou, Z.H., Zhang, K.L., Li, J., et al., 2006. Finite element analysis of stress and contact pressure on the rubber sealing O-ring. Lubr. Eng. 48 (4), 31–43.
Zhu, H.Y., Liu, Q.Y., Wong, G.R., et al., 2013. A pressure and temperature preservation system for gas-hydrate-bearing sediments sampler. Petrol. Sci. Technol. 31 (6), 652–662. https://doi.org/10.1080/10916466.2010.531352.